Available online at www.sciencedirect.com

SciVerse ScienceDirect

Journal of the European Ceramic Society 32 (2012) 425–431

www.elsevier.com/locate/jeurceramsoc

Oxygenation kinetics of YBCO-TSMG samples using the nanoindentation technique

J.J. Roa [a,*], F.T. Dias [b], M. Martínez [c], J.A. Padilla [c], M. Segarra [c]

[a] *Institut P', UPR 3346 CNRS-Université de Poitiers-ENSMA. Département de Physique et Mécanique des Matériaux., 86962 Futuroscope Chasseneuil Cedex, France*

[b] *Federal University of Pelotas, Physics and Mathematics Institute, Department of Physics, CP 354, 96010-900 Pelotas, Brazil*

[c] *DIOPMA Centre, Universitat de Barcelona, Faculty of Chemistry, Department of Materials Science and Metallurgical Engineering, C/Martí i Franquès, 1, E-08028 Barcelona, Spain*

Received 31 May 2011; received in revised form 31 August 2011; accepted 12 September 2011
Available online 6 October 2011

Abstract

Since hardness is a quantitative measure of bulk mechanical properties, it can be used to examine the kinetics of crack propagation inside $YBa_2Cu_3O_{7-\delta}$ (YBCO or Y-123) ceramics. YBCO samples with a tetragonal phase were oxygenated at a range of temperatures (from 250 °C to 750 °C) for different times. For each oxygenation temperature and time, hardness was measured by the nanoindentation technique, to study the defects (macro-/microcracks and porosity) produced along the *c*-axis. These defects were visualized by optical microscopy. The main purpose of this study was to establish the oxygenation kinetics for YBCO samples, which were textured by the top-seeded melt growth technique. We studied the evolution of hardness perpendicular to the *ab*-plane, as measured by the nanoindentation technique at a maximum penetration depth of 150 nm. The results indicate that the nanoindentation technique can be used successfully to monitor oxygenation and to establish the kinetics of the process.

Keywords: Superconductivity; Mechanical properties; Hardness; Oxide superconductors

1. Introduction

The oxygen content of the $YBa_2Cu_3O_{7-\delta}$ (YBCO or Y-123) single-domain bulk is related to its superconducting properties.[1] YBCO exhibits a tetragonal to orthorhombic (T-to-O) phase transformation as the oxygen content $(7-\delta)$ exceeds 6.5.[2] YBCO prepared by the top-seeded melt growth technique (TSMG)[3] contains cracks on the *ab*-plane (0 0 1). These cracks are often generated by volume changes during the T-to-O phase transition. These macro-/microcracks are highly undesirable in fundamental studies and engineering applications. Two types of macro-/microcrack are formed:

i. *a*/*b* macro-/microcracks parallel to the *a*/*b*-plane and
ii. *c* macro-/microcracks parallel to the *a*/*c*-plane.

While the *a*/*b* macro-/microcracks extend over almost the whole sample, the length of the *c*-macrocracks is limited by the spacing between the *a*/*b*-macrocracks.[4] The *c*-axis macrocrack network is a mesoscopic defect in bulk superconductors obtained by TSMG, and limits the local current density in the sample. Diko et al.[4] attributed microcracking to thermal expansion stresses between oxidized and non-oxidized zones. In addition, Reddy and Rajasekharan[5] studied the inner structure of partially oxygenated Y-123 bulk melt-textured material.

Nanoindentation, or the instrumented indentation technique (ITT) is a powerful tool for measuring mechanical properties at very small scales, mainly in the submicron range.[6] This is a versatile, non-destructive and selective technique. It can work at different applied loads, from 50 nN up to 500 mN. Nowadays,

* Corresponding author.
E-mail address: jjrr_cons@hotmail.com (J.J. Roa).

0955-2219/$ – see front matter © 2011 Elsevier Ltd. All rights reserved.
doi:10.1016/j.jeurceramsoc.2011.09.013

nanoindentation is commonly used for the mechanical characterization of thin films,[7] surface layers and bulk materials. One of the advantages of nanoindentation is that most of the mechanical properties of materials can be directly extracted from the analysis of the indentation load–displacement data (P–h curve), thus avoiding the need to observe the hardness imprint, and facilitating a proper measurement at sub-micron scale. Besides, the measurements are non-destructive at very small penetration depths. To our knowledge, there are no references to the determination of the oxygenation kinetics in YBCO materials using nanoindentation.

Here we used nanoindentation to examine the oxygenation kinetics of YBCO single domain samples in the direction perpendicular to the *ab*-plane. In addition, a SQUID magnetometer was used to measure the critical temperature (T_c) and the critical current density (J_c) for samples annealed at 450 °C.

2. Experimental procedures

2.1. Sample preparation

The samples were obtained by the TSMG technique.[8] A small $NdBa_2Cu_3O_{7-\delta}$ (NdBCO) melt-textured single domain was used as a seed. It was placed at the top centre of the pellet surface before heating, and the melt-growth process was performed. Before annealing under oxygen, the textured samples were cut from the middle part of the TSMG sample with the following dimensions: *width* = 4 mm, *length* = 4 mm and *height* = 4 mm. The samples were then introduced into a horizontal furnace at different temperatures (250, 350, 450, 550 and 750 °C) with a continuous oxygen flow of 0.2 ml/min, with 99.999% purity.

After the oxygenation process, the annealed samples were polished until half their initial width in order to examine the oxygenation profile before performing the mechanical characterization by nanoindentation. The structure of all polished samples was observed by optical microscopy with polarized light. Samples were etched in a solution of 1% (w/w) HCl in ethyl alcohol, to observe the several macro-/microcracks that had developed during the oxygenation process.

2.2. Mechanical tests

Hardness (H) tests were carried out in the direction perpendicular to the *ab*-plane, (Fig. 1). TSMG textured YBCO samples were tested using a Nanoindenter® XP System (Agilent Technologies) equipped with Test Works 4 Professional level software. A three-sided pyramid Berkovich diamond tip indenter was used. The displacement or penetration depth (h) was continuously monitored and load-time track of indentation was recorded. Indentations were made to a maximum depth of 150 nm, under a constant deformation rate of 0.05 s^{-1}. The Berkovich tip was calibrated with standard fused silica. In order to establish the kinetics of oxygenation by nanoindentation, the variation of the H values along 4 mm in the transversal direction of the *c*-axis was studied. The gap between imprints was 25 times the maximum penetration depth in order to isolate the plastic behaviour generated around the residual imprint. Eight hundred indentations were performed in the direction perpendicular to the *ab*-plane of each sample, in order to obtain an internal hardness profile. Based on the experimental results, the H values were calculated as a function of penetration depth using the Oliver and Pharr approach.[9] In this method, the contact depth (h_c) is expressed as:

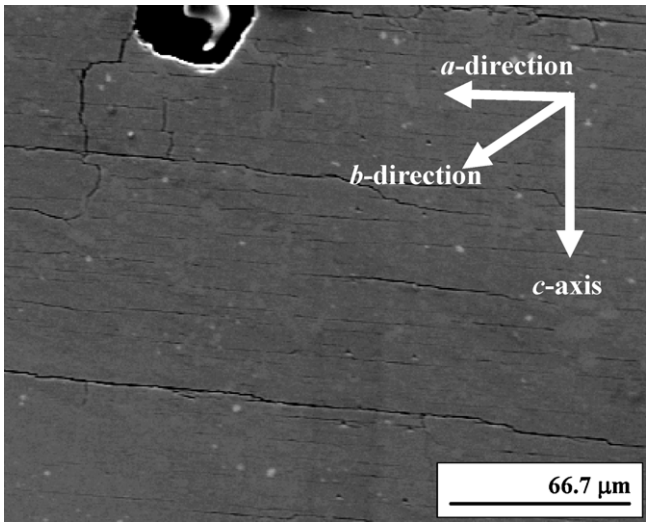

Fig. 1. FE-SEM micrograph of the *c*-axis of a YBCO textured sample after oxygenation.

$$h_c = h_{max} - \varepsilon \frac{P_{max}}{S} \quad (1)$$

where ε is a parameter equal to 0.75 for a Berkovich tip indenter, h_{max} is the maximum penetration depth, P_{max} is the maximum applied load, and S is the contact stiffness. The main parameter used to determine the H value is the contact area, $A(h_c)$, which is calculated using the shape factor of the indenter. The H value is calculated by:

$$H = \frac{P_{max}}{A(h_c)} = \frac{P_{max}}{24.5 h_c^2} \quad (2)$$

2.3. Superconducting characterization

A *dc* magnetization measurement was made using a superconducting quantum interference device SQUID MPMS-XL magnetometer from Quantum Design. The method consists of cooling the sample to below T_c in zero field cool (ZFC). Then, the magnetization is measured under a constant magnetic field of 10 Oe along the *c*-axis while the sample is slowly warmed to above T_c. Subsequently, the magnetization is measured while the sample is cooled to below T_c in the same field cool (FC). The critical temperature and the irreversible behaviour of magnetization can be identified with this procedure.

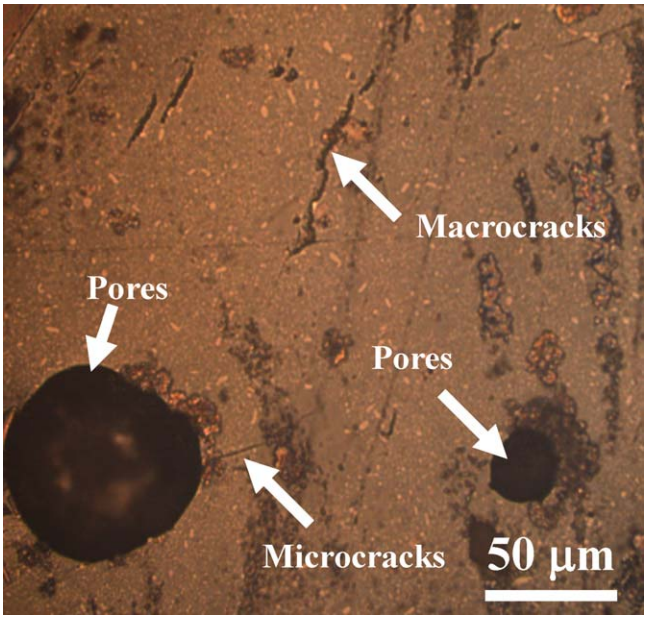

Fig. 2. Optical image of a region of the same sample with a high pore density generated during oxygenation.

3. Results and discussion

3.1. Oxygen defects and macro-/microcracking in melt-textured samples

The *c*-axis section of the oxygenated samples was examined in order to detect the tetragonal regions, which can be clearly distinguished under polarized light as dark or bright regions depending on the orientation of the Y-123 crystal axes.[10] Macro- and microcracking were the main structural changes observed in the samples after oxygenation, (Fig. 2). Moreover, the pores created during the melting process tended to grow during oxygenation due to the movement of these macro-/microcracks. Both defects make the samples more brittle, as a consequence of the structural change. Moreover, Y-211 phase has a lower thermal expansion coefficient than Y-123 phase in the *c*-direction,[11–14] therefore Y-211 particles are under tension during cooling, and *a*/*b*-macro-/microcracking is enhanced. Additional tensile stresses in the *c*-growth section (GS) tends to enlarge *a*/*b*-macro-/microckracks. The length and width of *a*/*b*- and *c*-macro-/microcracks increase continuously with the oxygenation temperature. At higher oxygenation temperatures, the width of *a*/*b*-, and especially the *c*-macro-/microcracks, increases significantly. In contrast, at lower oxygenation temperatures (such as 450 °C) the *c*-macrocracks are fine and their density in the sample is high. Tensile stresses in the *c*- and a/b-direction are induced by shrinkage of the lattice parameters of the Y-123 phase with oxygen content. These stresses are therefore responsible for *a*/*b*- and *c*-crack formation in the oxygenated layer. Oxygen may then flow along the *c*-cracks to the *a*/*c*-surfaces, oxygenating the surface and tip of the *c*-cracks and furthering their propagation. As can be seen in Figs. 1 and 2, a high crack density is generated during the T-to-O transition due to the stress provided by the volume change. As the *c*-axis shortens, the Y-211 particles distributed in the matrix remain elastically rigid and prevent the YBCO crystal from deforming. This tensile stress is concentrated near the Y-211 particles. In order for these cracks to propagate, several conditions are required:

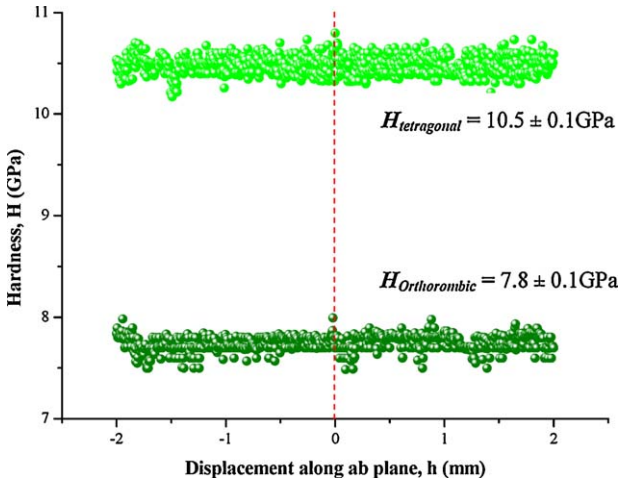

Fig. 3. Nanohardness evolution on the *a*/*b*-plane of tetragonal and orthorhombic phases along the *c*-axis.

i. there must be oxygen inhomogeneity in the sample,
ii. the sample must have a minimum size in which enough volume stress can be generated during this process,
iii. an isotropic second phase must exist, to convert the compressive stress into tensile stress due to the *c*-axis shortening, and
iv. a T-to-O phase boundary must exist.

As oxygen diffuses into the single domain, the first profile established at the surface is the one where the oxygen level is the highest. As the oxygen content rises above 6.5, the T-to-O phase transition takes place.[15] When the oxygen content reaches a constant value, the cracks have propagated throughout the entire crystal, and no further cracks are generated.

3.2. Oxygenation kinetics

The hardness of the tetragonal and orthorhombic phases was measured respectively in non-oxygenated and in fully oxygenated melt-textured YBCO samples, in order to provide reference values before the oxygenation process. Fig. 3 shows the nanohardness values of the reference samples across the *c*-axis. In this figure, 0 *x*-axis is the centre of the sample. The results obtained for each phase across the *c*-axis are: $H_{\text{tetragonal}} = 10.5 \pm 0.1$ GPa and $H_{\text{orthorombic}} = 7.8 \pm 0.1$ GPa. These values are consistent with a previous report for a different sample,[16] in which $H_{\text{tetragona}} = 10.6 \pm 0.4$ GPa and $H_{\text{orthorombic}} = 7.6 \pm 0.4$ GPa.

As a result of the T-to-O phase transition, structural changes leads to the formation of various lattice defects such as twinning and microcracks. These defects have significant effects on physical properties including flux pinning and current density

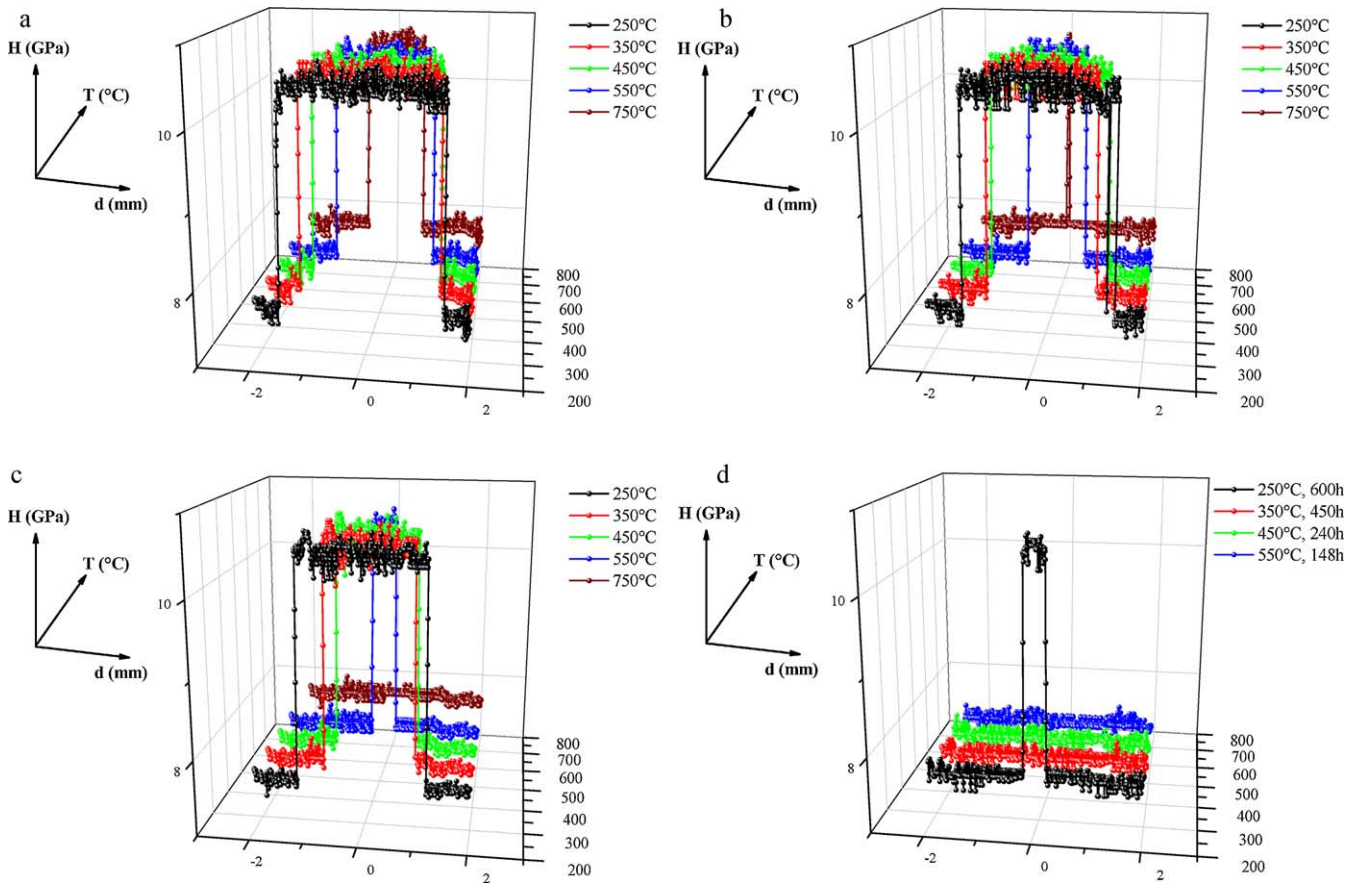

Fig. 4. Hardness evolution at different oxygenation temperatures and at different times. (a) 24 h, (b) 48 h, (c) 72 h, and (d) longer oxygenation times. Where H is the hardness and T is the temperature.

transport in the YBCO crystals.[17] One of the negative consequences of the T-to-O transition is the formation and propagation of macro-/microcracks along the *a*/*b*-plane. When the phase transition takes place, the *c*-axis becomes shorter, thus creating tensile stress in the outer regions of the sample. This strain profile at the oxygenation layer produces cracks parallel to *a*/*b*-plane,[11,18] although the contraction of the crystal along the *c*-axis is hindered by the Y-211.[15,19,20]

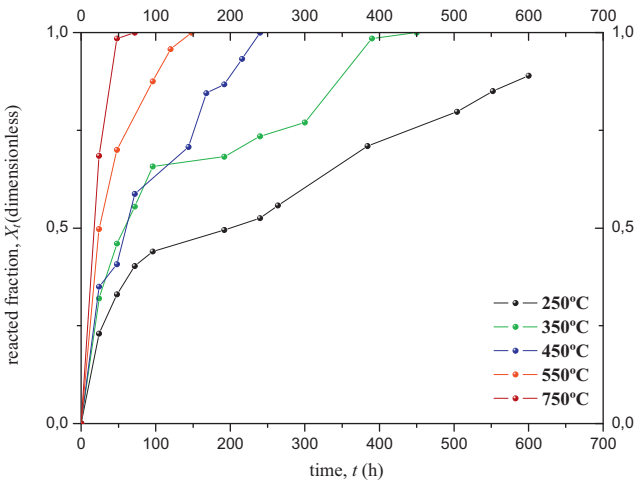

Fig. 5. Reacted fraction versus time plot at different oxygenation temperatures.

Upon crack formation, oxygen diffusion accelerates along the crack. As the oxygen diffuses into the sample along the *c*-axis, these microcracks also propagate towards the core of the domain structure at a rate that is comparable to oxygen diffusion. Fig. 4 shows the hardness evolution at different oxygenation temperatures and times in the direction perpendicular to the *a*/*b*-plane. As can be seen for each temperature, the hardness decreases progressively at both extremes of the sample when the oxygenation time increases. In this figure, we can see that the oxygenation process for YBCO-TSMG samples is symmetrical. At longer oxygenation times, all the samples are completely transformed from tetragonal to orthorhombic phase, except when oxygenated at 250 °C for 600 h (Fig. 4d).

In order to study the kinetics of the process, the reacted fraction at each time point was calculated from the following expression:

$$X_t = \frac{h_{\text{tetragonal}\rightarrow\text{Orthorombic}}}{w_{\text{sample}}/2} \tag{3}$$

where $h_{\text{tetragonal}\rightarrow\text{orthorombic}}$ corresponds to the distance of the oxygenation front from the centre where the change in hardness is observed in all the measurements performed on YBCO samples in the direction perpendicular to the *c*-axis, and w_{sample} is

the width of the sample. The oxygenation rate was calculated from the following expression:

$$r = \frac{dX_t}{dt} \quad (4)$$

Fig. 5 shows conversion of the transformed phase at each time (X_t) versus oxygenation time (t) at different temperatures.

There are two types of reaction between solids and fluids: those in which the solid size does not appear to vary, as the characteristics of the products are similar to that of the initial solid, and those in which the initial solid shrinks, as the result of the formation of a gas product, for example.

For non-catalytic solid–fluid reactions, different kinetic models can be considered: shrinking core, shrinking particle, homogeneous and grain models. In the shrinking core model (SCM) a non-porous solid is considered whose external surface is the first to react. Afterwards, the reaction front moves inwards the solid, leaving behind the fully converted material. An un-reacted core remains, whose size decreases as the reaction proceeds. The shrinking particle model is similar to the SCM except that no product layer is left around the un-reacted core. The homogeneous model is applicable to a solid with a homogeneous distribution of pores, while the grain model is applicable to a solid consisting of individual dense grains compacted together.

For solids with low porosity, the most realistic model to represent the reaction between a fluid and a solid is the shrinking core model.[21]

The SCM was first developed by Yagi and Kunii,[22] and it considers the solid reactant as non-porous and initially surrounded by a fluid film through which mass transfer occurs between the solid particle and the bulk of the fluid. As the reaction proceeds, a product layer forms around the un-reacted core.

The reaction rate is determined by the control regime, that is the rate-limiting step. If it is assumed that the solid particle is spherical, that it reacts with the fluid isothermally, and also that the concentration of the reacting fluid is constant or in excess, depending on the rate-limiting step, the reacted fraction (X_t) can be expressed by the following equations:

- When the process is controlled by the diffusion through the fluid layer surrounding the solid particle:

$$X_t = k_f t \quad (5)$$

where k_f is a constant that includes the concentration of reactants and the density of the solids.

- When the process is controlled by the diffusion through the solid products layer:

$$1 - 3(1 - X_t)^{2/3} + 2(1 - X_t) = k_d t \quad (6)$$

where k_d is a constant proportional to the diffusion coefficient.

- When the process is controlled by the chemical reaction at the surface of the un-reacted core:

$$1 - (1 - X_t)^{1/3} = k_r t \quad (7)$$

where k_r is a constant that includes the concentration of reactants and the density of the solids.

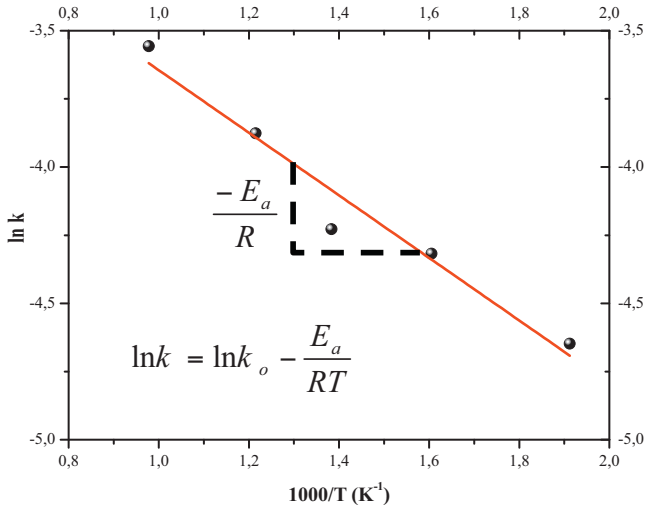

Fig. 6. Arrhenius plot.

If we plot the three left terms of these equations against time, none of them gives us a straight line, thus indicating that two or more process steps overlap in the oxygenation of YBCO-TSMG and that the rate-controling process changes as the reaction proceeds.

If we plot the logarithm of the initial reaction rate (that is the slope of each curve in Fig. 5 at time zero), versus the inverse of the temperature, we can calculate the activation energy of the first process taking place. Thus, Fig. 6 shows the Arrhenius plot. The activation energy, calculated for annealing times shorter than 50 h, is 9.5 kJ/mol, thus indicating that the initial process is controlled by oxygen diffusion. This energy can be considered as the minimum energy necessary to begin the T-to-O phase transition.

The first stage of the oxygenation process can be related to the diffusion of oxygen into the sample, favored by the microcracks produced during crystal growth. Once oxygen reaches the surface, it reacts with the tetragonal phase, leading to the orthorhombic phase. This generates an important change in volume that is translated into the formation of more cracks, which increase the reactive surface. So, the first initial step can be modeled by a typical diffusion equation, while the T-to-O transition can be modeled by reaction rate-controlled kinetics, as it increases the oxygen diffusion, thus becoming the restrictive stage. Consequently, crack formation mainly depends on the diffusivity of oxygen.[15] At higher temperatures, at which oxygen diffusion is more favored, only one curve is observed related to the reaction rate-controlled stage. Thus, the combination of both processes in series would yield this particular plot.

3.3. Determination of the magnetic properties by SQUID

At annealing times around 182 h at 450 °C, as indicated by the nanoindentation results (Fig. 4c), the oxygenation content of the sample is quite homogeneous. Fig. 7a and b shows a typical magnetization curve for YBCO samples annealed at 450 °C for 182 h and 240 h, respectively. Due to the low magnetic field applied in this case, the critical temperature (Tc) can be determined by

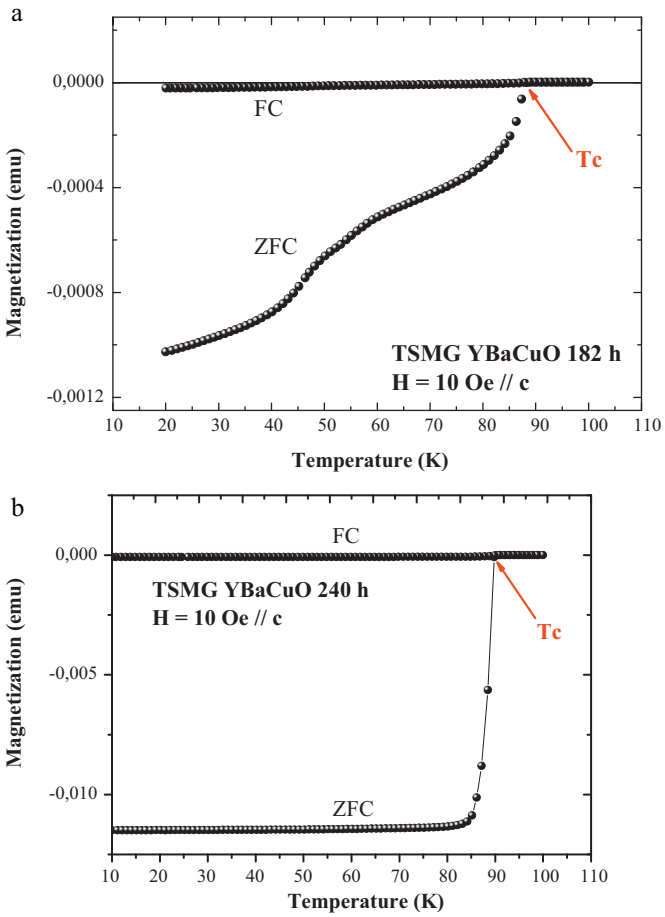

Fig. 7. Magnetization versus temperature at of 450 °C. (a) 182 h and (b) 240 h.

the intersection of ZFC and FC curves, as shown in Fig. 7a, which occurs at 88 K. The superconducting transition presented is very large and occurs in a two-step process. This phenomenon is attributed to the fact that the oxygenation time (182 h) was not long enough to produce the full transition from tetragonal to orthorhombic phase and conversion was incomplete. However, after 240 h of annealing, the magnetization results show a narrow transition, with only a one-step process, and with higher magnetic shielding values (see ZFC curve) than in the previous case (182 h), although the Tc is similar in both cases. This case corresponds to the complete T-to-O transition of the overall sample (Fig. 5).

4. Conclusions

Nanoindentation has been shown to be a powerful tool to characterize the mechanical stability and determine the kinetics of oxygenation of YBCO-TSMG samples. We determined the variation of the hardness along the *c*-axis at different oxygenation times.

The oxygenation process induces micro- and macrocracks due to the introduction of oxygen atoms inside the crystallographic structure. Moreover, we found that the oxygenation process is mainly controlled by the oxygen diffusion at low temperatures. During the first 50 h the oxygen enters the structure through microcracks produced during the texturing process. After this time, the T-to-O transition takes place, thus producing an important change in volume, leading to more microcracks that increase the reactive surface.

The activation energy for the first stage of the oxygenation of the superconducting samples was found to be 9.5 kJ/mol.

Acknowledgment

We would like to thank the Linguistic Services at the Universitat de Barcelona for linguistic and stylistic advice.

References

1. Zheng MH, Xiao L, Ren HT, Jiao YL, Chen YX. Study of oxygenation process during the preparation of single domain YBCO bulk superconductors. *Physica C* 2003;**386**:258–61.
2. Shi D, Chaud X, Odier P, Sulpice A, Isfort D, Tournier R, et al. Modulus study of microcracks in single domain $YBa_2Cu_3O_x$ with *c*-axis pressure during oxygen anneal. *Physica C* 2006;**443**:18–22.
3. Shi D, Isfort D, Chaud X, Odier P, Mast D, Tournier R. Suppression of *ab*-plane crack formation in single domain $YBa_2Cu_3O_x$ by uniaxial *c*-axis pressure. *Physica C* 2004;**402**:72–9.
4. Diko P, Krabbes G. Formation of c-macrocracks during oxygenation of TSMG $YBa_2Cu_3O_7/Y_2BaCuO_5$ single-grain superconductors. *Physica C* 2003;**399**:151–7.
5. Reddy ES, Rajasekharan T. Nucleation and growth of the orthorhombic phase in melt textured $YBa_2Cu_3O_{6+\delta}$. *Physica C* 1997;**279**:56–62.
6. Roa JJ, Capdevila XG, Martínez M, Espiell F, Segarra M. Nanohardness and Young's modulus of YBCO samples textured by the Bridgman technique. *Nanotechnology* 2007;**18**, 38501/1–6.
7. Roa JJ, Gilioli E, Bissoli F, Pattini F, Rampino S, Capdevila XG, et al. Study of the mechanical properties of CeO_2 layers with the nanoindentation technique. *Thin Solid Films* 2009;**518**:227–32.
8. Cima MJ, Flemings MC, Figueredo AM, Nakade M, Ishii H, Brody HD, et al. Semisolid solidification of high temperature superconducting oxides. *Journal Applied Physics* 1992;**72**:179–90.
9. Oliver W, Pharr G. An improved technique for determining hardness and elastic modulus using load and displacement sensing indentation experiments. *Journal of Material Research* 1992;**7**:1564–83.
10. Diko P, Gawalek W, Habisreuther T, Klupsch Th, Görnet P. Macro- and microcracking subgrains, twins and thermal stresses in $YBa_2Cu_3O_{7-x}$ (123)–Y_2CaCuO_5 (211) melt textured superconductors studied by means of polarized light microscopy. *Journal of Microscopic* 1996;**184**:46–57.
11. Diko P, Krabbes G. Macrocracking in melt-growth YBaCuO superconductor induced by surface oxygenation. *Superconductor Science and Technology* 2003;**16**:90–3.
12. Okudera T, Murakami A, Katagiri K, Kasaba K, Shoji Y, Noto K, et al. Fracture toughness evaluation of YBCO bulk superconductor. *Physica C* 2003;**392**:628–33.
13. Raynes AS, Freiman SW, Gayle FW, Kaiser DL. Fracture toughness of $YBa_2Cu_3O_{6+\delta}$ single crystals: anisotropy and twinning effects. *Journal of Applied Physics* 1991;**70**:5254–7.
14. Diko P. Cracking in Melt-Processed RE–Ba–Cu–O Superconductors. *Superconductor Science and Technology* 1998;**11**:68–72.
15. Shi D, Odier P, Sulpice A, Isfort D, Chaud X, Tournier R, et al. Kinetics study of *ab*-plane crack propagation by modulus measurement in single domain $YBa_2Cu_3O_x$. *Physica C* 2003;**384**:149–58.
16. Bartolomé E, Roa JJ, Bozzo B, Segarra M, Granados X. Effective silver-assisted welding of YBCO blocks: mechanical versus electrical properties. *Superconductor Science and Technology* 2010;**23**, 045013/1–6.
17. Liang R, Bonn DA, Hardy WN. Growth of high quality YBCO single crystals using $BaZrO_3$ crucibles. *Physica C* 1998;**304**:105–11.

18. Isfort D, Chaud X, Tournier R, Kapelski G. Cracking and oxygenation of YBaCuO bulk superconductors: application to *c*-axis elements for current limitation. *Physica C* 2003;**390**:341–55.
19. Shi D, Lahiri K, Qu D, Sagar S, Solovjov VF, Pan VM. Surface nucleation, domain growth mechanisms, and factors dominating superconducting properties in seeded melt growth $YBa_2Cu_3O_x$. *Journal of Materials Research* 1997;**12**:3036–45.
20. Li Y, Zdun K, Hope L, Xie J, Corcoran S, Qiao Y, et al. Texture development and superconducting properties of YBCO thick films deposited on buffered metal substrates at various deposition rates. *IEEE Transaction on Applied Superconductivity* 2003;**13**(2):2758–61.
21. Izquierdo JF, Cunill F, Tejero J, Iborra M, Fite C. *Cinetica de las reacciones químicas*. Barcelona: Edicions Universitat de Barcelona; 2004, ISBN 84-8338-479-5.
22. Yagi S, Kunii D. Studies on combustion of carbon particles in flames and fluidized beds. In: *Fifth Symposium (International) on Combustion*. 1955. p. 231–44.